Direct Observation of the Electrically Triggered Insulator-Metal Transition in V_3O_5 Far below the Transition Temperature

Coline Adda,[1,*] Min-Han Lee,[1,2] Yoav Kalcheim,[1,†] Pavel Salev,[1] Rodolfo Rocco,[3] Nicolas M. Vargas,[1] Nareg Ghazikhanian,[1,2] Chung-Pang Li,[4] Grant Albright,[4] Marcelo Rozenberg,[3] and Ivan K. Schuller[1]

[1]*Department of Physics and Center for Advanced Nanoscience, University of California-San Diego, La Jolla, California 92093, USA*

[2]*Materials Science and Engineering Program, University of California-San Diego, La Jolla, California 92093, USA*

[3]*Université Paris-Saclay, CNRS, Laboratoire de Physique des Solides, 91405, Orsay, France*

[4]*Quantum Focus Instrument, Vista, California 92081, USA*

(Received 28 January 2021; revised 10 August 2021; accepted 29 November 2021; published 7 February 2022)

Resistive switching is of the key phenomena for applications such as nonvolatile memories or neuromorphic computing. V_3O_5, a compound of the vanadium oxide Magnéli series, is one of the rare materials to exhibit an insulator-metal transition above room temperature ($T_c \sim 415$ K). The switching mechanisms in this material are still not clear. Here, we demonstrate both static dc volatile resistive switching and fast oscillatory spiking regimes in V_3O_5 devices at room temperature (120 K below the phase transition temperature) by applying an electric field. We couple electrical measurements, *operando* optical imaging, and infrared measurements to track the reflectivity change and the temperature of a device during the resistive switching. We find that the resistive switching starts via thermal runaway deep in the insulating state and triggers the phase transition with the formation of a filament of the high-temperature phase. Furthermore, we capture optically and thermally the spiking oscillations that we link to the negative differential resistance regime and find the filament forms and dissolves via a periodic spatiotemporal instability that we describe by numerical simulations. Our studies play an important role in understanding the volatile resistive switching mechanisms and demonstrate that V_3O_5 can be a key vanadium oxide for neuromorphic computing.

DOI: 10.1103/PhysRevX.12.011025

Subject Areas: Condensed Matter Physics
Materials Science

Resistive switching (RS) in materials that undergo an insulator-to-metal phase transition (IMT) is the subject of intense fundamental research [1–5] and could enable a variety of novel applications, ranging from optoelectronic devices [6–9] to artificial neurons and synapses for hardware-level neuromorphic computing [10–15]. Two distinct types of RS are possible in IMT materials [16]: nonvolatile (NVRS) and volatile (VRS). In NVRS, the resistance change induced by the voltage application persists after the voltage is turned off. Typically, NVRS is due to electrically stimulated ionic migration. In materials such as $(Pr, Ca)MnO_3$ [17] and $(RE)NiO_3$ [18], the ionic migration can locally change the doping level, prompting an IMT and causing RS. Even a subtle chemical modification can produce orders of magnitude resistance change, presenting an advantage of the IMT materials over conventional binary oxide memristors. For VRS, which this paper focuses on, the resistance change is also induced by the application of voltage; however, the material automatically "resets" into the initial state when the voltage is turned off. The VRS often manifests as the appearance of a negative differential resistance (NDR) in the I-V characteristics, i.e., a region where the slope dV/dI is negative. VRS most commonly can be induced in IMT materials that feature a temperature-dependent phase transition.

From an applied point of view, room-temperature operation of devices is highly desirable. The number of materials with the IMT above room temperature, however, is rather limited [19]. At present, most research on volatile resistive switching focuses in VO_2 ($T_c \approx 340$ K) and NbO_2 ($T_c \approx 1080$ K). When volatile resistive switching is

*Corresponding author.
cadda@physics.ucsd.edu

†Present address: Faculty of Materials Science and Engineering, Technion—Israel Institute of Technology, Haifa 32000, Israel.

realized at temperatures far below the phase transition temperature, it is not always clear whether or how the switching is related to the phase transition. Several explanations for the origin of the resistive switching have been proposed: triggering of the IMT by Joule heating, doping of the insulating phase by the field effect, and the so-called "thermal runaway." In the first case, the electrical triggering of the IMT by Joule self-heating leads to the formation of a high-temperature phase metallic filament [5,20]. In the second case, the high electric field promotes charges from a low-energy state into the conduction band, thus electrically doping and destabilizing the Mott state [2,3,21,22]. Thermal runaway occurs by the formation of a low-resistance filament at an intermediate temperature (that is below the temperature of the high-temperature metallic phase), which is possible because of a rapid decrease of resistance with increasing temperature in the insulating phase.

It is well established that the switching in pristine VO_2 [3,5,20] at room temperature (i.e., ∼50 K below T_c) can be driven by local Joule heating across the IMT. On the other hand, in V_2O_3 (and also radiation-damaged VO_2), resistive switching can be accomplished by destabilization of the Mott state by charge injection [3]. In NbO_2, volatile resistive switching at room temperature (i.e., ∼790 K below T_c) has been claimed as the consequence of both local heating across the IMT [23,24] and thermal runaway [25–28] and, therefore, might be a result of Joule heating. The variety of possibilities illustrates that observation of resistive switching in an IMT material does not automatically indicate the switching mechanism. Therefore, careful assessment of the experimental evidence including local phase and local temperature distributions becomes necessary to unravel the origin of the VRS in IMT materials, especially when the switching is triggered far below the transition temperature.

In this work, we explore the physical origin of the room-temperature VRS in V_3O_5 thin films. V_3O_5 is a member of the vanadium oxide Magnéli series, and it has an IMT occurring around $T_c \approx 420$ K [29]. The IMT is accompanied by a large resistivity change and a subtle structural modification [30,31]: Monoclinic V_3O_5 lattice transforms between the space groups $P2/c$ ($T < T_c$) and $I2/C$ ($T > T_c$). The absence of a pronounced structural transition in V_3O_5 presents a considerable advantage for applications, as a repeated triggering of the IMT should not lead to a buildup of large internal strain (unlike VO_2, for example, in which approximately 1% strain can arise during the transition [32,33]). The continuous change of resistivity across the IMT and the absence of a noticeable thermal hysteresis suggest that the phase transition is of the second order [34,35]. The low-temperature insulating state in V_3O_5 is often attributed to the ordering of V^{3+} and V^{4+} ions below T_c, which is proposed to be the consequence of electron-electron Coulomb interactions and of electron-phonon coupling (i.e., polaron formation) [35–37]. Above T_c, electrons can hop between V^{3+} and V^{4+} ions, leading to a poor metallic state characterized by a short electron mean free path and by a low carrier mobility [37].

The IMT in V_3O_5 can be induced by a variety of external stimuli other than temperature, such as pressure [38], light [35,39], and voltage [40]. The latter is demonstrated to produce VRS in bulk crystals at room temperature (i.e., 120 K below T_c), which is attributed to Joule self-heating. No direct evidence, however, is presented on whether the switching is caused by inducing the IMT thermally by self-heating to T_c or by a thermal runaway resulting in the formation of a "hot" low-resistance filament across an otherwise insulating phase. Here, we combine electrical switching with optical reflectivity (sensitive to metal-insulator phase) and midwave infrared (MWIR) emission (sensitive to temperature) imaging techniques to gain definitive insight on the mechanism. We show that the VRS combines the features of two mechanisms. The switching is initiated by a thermal runaway deep within the insulating phase because of the steep resistance vs temperature dependence. The thermal runaway then triggers the IMT, stabilizing a filamentary conductive path consisting of the high-temperature phase, which crucially quenches a further runaway and preserves the device from thermal degradation. We observe this two-stage process both in static dc switching measurements and in the dynamic self-oscillating regime. These conclusions and the details of the switching mechanism are supported by resistor network simulations. Our results directly show that an IMT could be triggered electrically at temperatures far below T_c.

The synthesis of pure phase V_3O_5 is challenging, because the required stoichiometric range is very narrow ($VO_{1.666}$; $VO_{1.668\pm0.002}$) [39,41]. In this work, we synthesize V_3O_5 films by transforming V_2O_3 films using a unique gas evolution technique with a precise control of a high-temperature oxygen-rich environment [42]. Ti/Au electrodes 20 μm wide and separated by a 20 μm gap are patterned on top of the film to make planar two-terminal devices for resistive switching measurements. The planar device configuration enables easy access to probe the IR emission or optical response of V_3O_5 simultaneously with the electrical properties, which allows us to monitor the temperature and to detect the triggering of the phase transition during resistive switching.

We observe a clear signature of the phase transition in our V_3O_5, by using two independent techniques, resistance (R) and optical reflectivity (Ref) vs temperature measurements [Figs. 1(a) and 1(b)]. Around $T_c \approx 415$ K, the resistance rapidly changes by about a factor of 3. At the same time, the devices display a significant reduction in their optical reflectivity. Both $R(T)$ and $\mathrm{Ref}(T)$ show a continuous, nonhysteretic evolution near T_c, which is

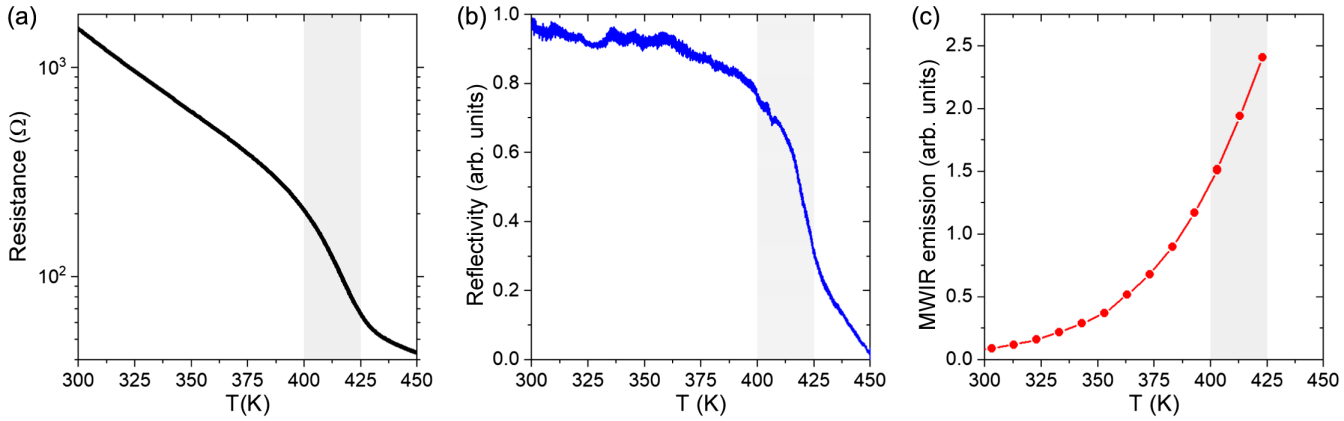

FIG. 1. Equilibrium properties of V_3O_5. (a) The resistance vs temperature [$R(T)$] and (b) the reflectivity vs temperature [$\mathrm{Ref}(T)$] curves clearly show an IMT around 415 K (gray area). No thermal hysteresis can be observed in either curve, indicating a second-order phase transition. (c) Infrared (MWIR) emission vs temperature showing steady monotonic increase. No anomalous behavior in the vicinity of the IMT can be observed in the IR signal.

expected for a second-order phase transition [34,35]. There is an important difference, however, between the $R(T)$ and $\mathrm{Ref}(T)$. The former shows a strong nonlinear (exponential) resistance decrease in the insulating state, below $T < 400$ K. Because of this, the relative resistance change from room temperature to the onset of the phase transition is comparable to the relative resistance change across the IMT. As a consequence, the observation of a resistance change during a switching experiment does not necessarily imply that T_c has been exceeded and that the phase transition has been triggered, making resistance an unreliable quantity for tracking the onset of the IMT.

In contrast, since the optical reflectivity is nearly temperature independent in the insulating state, the abrupt changes at the IMT onset imply that the IMT is triggered under the external stimuli. However, although the reflectivity is sensitive to the high-T phase, information about the temperature during the resistive switching, i.e., whether the IMT is caused by heating, is still missing. To address this issue, we measure the naturally emitted MWIR radiation by the device to quantify its temperature variation. Figure 1(c) shows the equilibrium IR emission of the V_3O_5 film (i.e., without application of a strong voltage or current). The data are recorded using a liquid-nitrogen-cooled InSb detector that detects the MWIR signal at around 5 μm wavelength. Because of the limited sensitivity bandwidth of the detector, the IR emission does not precisely follow the Stefan-Boltzmann law, i.e., T^4 dependence. The MWIR signal, however, shows a steady monotonic increase with increasing temperature. Importantly, the IR emission does not display an anomalous behavior in the vicinity of the IMT, which makes the IR measurements ideal for probing temperature. Therefore, combining optical reflectivity and IR emission measurements allows us to detect the phase transition and to quantify Joule heating during the VRS in V_3O_5.

V_3O_5 devices show pronounced resistive switching at room temperature. We observe [Fig. 2(a)] that, above a certain threshold, the current-controlled I-V characteristics develops an S-type negative differential resistance. The NDR first appears under a relatively large power (120 mW) dissipated in the device. Such large power is expected to cause significant Joule self-heating, which most likely drives the observed resistive switching. However, as discussed before, this observation alone does not permit to unambiguously determine whether the device has overcome the phase transition temperature. Another important observation is that the I-V characteristic does not show any significant hysteresis. This is in stark contrast with the previously reported measurements in V_3O_5 bulk crystals [40]. We attribute the absence of the I-V hysteresis in our devices to the thin film geometry. Good thermal coupling between the Al_2O_3 substrate and the V_3O_5 film leads to rapid establishment of a steady-state temperature distribution in the device upon changing the applied voltage or current. The efficient thermal coupling in thin film devices enables fast speed operation, which we demonstrate next by probing the self-oscillation regime in V_3O_5.

Inducing a dynamic self-oscillating resistive switching regime in IMT materials allows mimicking the spiking behavior of biological neurons, which could find applications in hardware-level implementation of neuromorphic computing [43,44]. We realize self-oscillation in V_3O_5 by assembling a Pearson-Anson-type circuit [Fig. 2(b)] [45]. We connect a series resistor and a parallel capacitor to the V_3O_5 device and monitor the instantaneous voltage and current using an oscilloscope. We observe fast current oscillations at room temperature when the circuit is biased using a dc voltage [Figs. 2(c)–2(e)]. The oscillation regime appears within a certain dc bias range that depends on the parallel capacitance value. The larger the capacitor, the

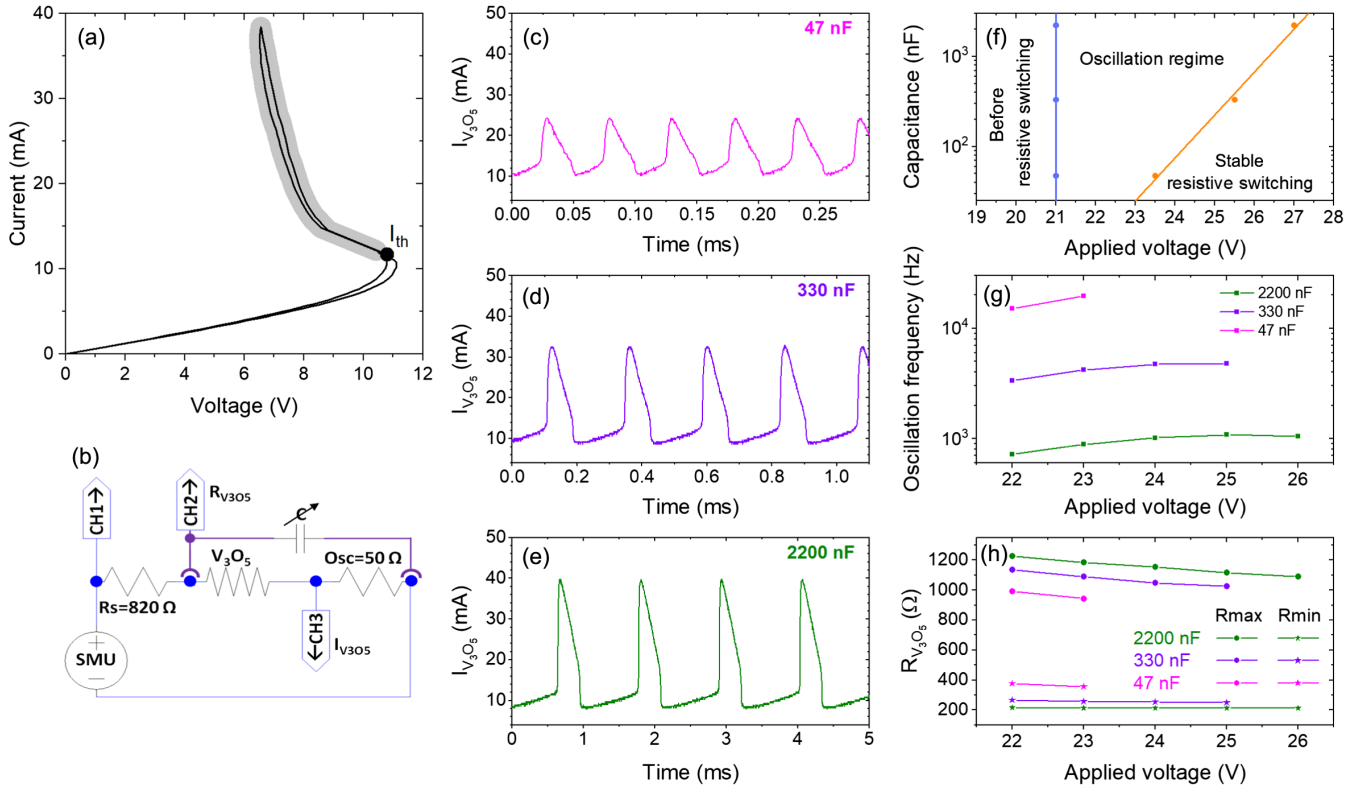

FIG. 2. Resistive switching and self-oscillation in V_3O_5. (a) RT current-voltage characteristic. Above approximately 12 mA threshold current, the V_3O_5 device switches into a low-resistance state as indicated by the appearance of an S-type NDR ($dV/dI < 0$) regime (gray shaded area in the *I-V* plot). (b) Pearson-Anson circuit used in the self-oscillation measurements. (c)–(e) Time dependence of the current through the V_3O_5 device for different capacitances: 47 nF in (a), 330 nF in (b), and 2200 nF in (c). (f) Summary of the three different regimes as a function of the capacitance and the applied voltage. For voltages below 21 V, the device is always insulating. Above 21 V, the device enters an oscillation regime that ends at higher voltages where the resistive switching state is stable. (g) Oscillation frequency as a function of the applied voltage for different capacitance. The frequency decreases as the capacitance increases but increases with the voltage. (h) Minimum and maximum resistances of the V_3O_5 device during the oscillation regime as a function of the voltage and for different capacitances. Both the amplitude of the resistance change and the extrema resistance values depend on the capacitance. The maximum resistance decreases slowly with the applied voltage independently of the capacitance, and the minimum resistance is nearly independent of the voltage.

wider the dc bias range in which the oscillating regime can be induced [Fig. 2(f)]. Outside this bias range, the device remains either in the insulating state when the bias is too small or in a nonoscillatory, stable low-resistance regime (similar to the dc *I-V*) when the bias is too large. Within the oscillatory regime, both the frequency [Fig. 2(g)] and amplitude [Fig. 2(h)] depend strongly on the capacitance. By adjusting the parallel capacitor, oscillations can be induced in the range from hundreds of hertz to several tens of kilohertz with amplitudes from 10 to 30 mA. Although the oscillation parameters can also be manipulated by the dc bias, their dependence is much weaker than the effect of changing the capacitor. The ability to drive V_3O_5 into the two resistive switching regimes, static dc switching and dynamic self-oscillations, provides the opportunity to study both quasiequilibrium switching properties and switching dynamics, which we investigate using the combination of optical and IR measurements.

We find clear evidence that VRS in V_3O_5 results from triggering the IMT, triggered by thermal runaway initiated deep in the insulating state. Figure 3 presents MWIR imaging performed during the resistive switching. This is obtained in a current-controlled mode at room temperature, using the optical reflectivity under white light illumination and the natural infrared emission. The optical images [Fig. 3(a)] are differential: We subtract images recorded under applied current from a reference image at zero current, which helps enhance the contrast. The MWIR thermal maps [Fig. 3(d)] are converted into temperature maps from raw MWIR emission images using equilibrium temperature IR emission images (i.e., without current or voltage applications) for the calibration. To facilitate the comparison between the data obtained in different instruments, we use a current normalized by I_{th}, the current at which the switching occurs (the onset of NDR). Unnormalized raw experimental data are available in Supplemental Material [46].

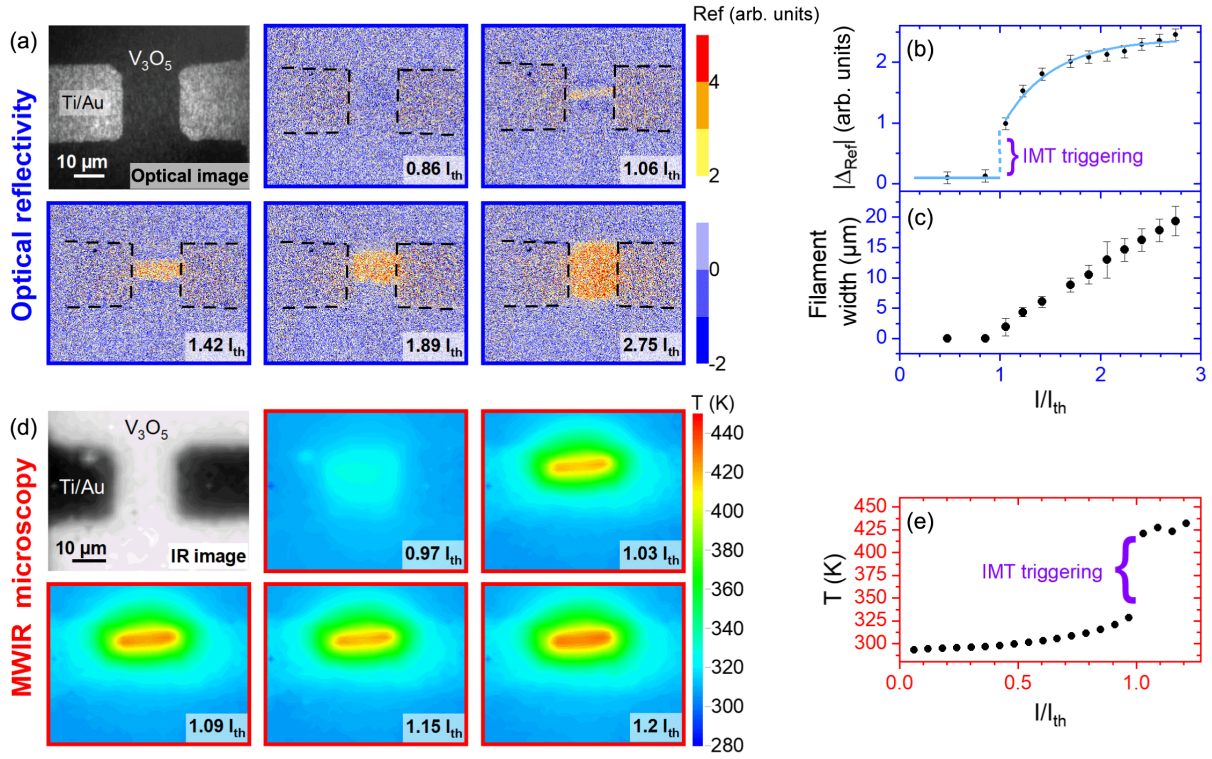

FIG. 3. Optical imaging and MWIR temperature mapping of the resistive switching in V_3O_5. (a) Optical image of the V_3O_5 device. The dark area is the V_3O_5 film; the two bright regions are the electrodes. The gap separating the two electrodes is approximately 20 μm. The differential contrast images of the resistive switching in V_3O_5 (see the main text for details) show the formation of the filament that percolates between the electrodes. The low-temperature phase is in blue, and the high-temperature phase is in orange. This filament is the high-temperature phase of V_3O_5. (b),(c) Reflectivity change and filament width vs normalized current extracted from the optical reflectivity images. (d) IR emission image of the V_3O_5 device (performed with a QFI Infrascope). Note that the contrast is reversed compared to the optical image in (a), which is due to low emissivity of the metal electrodes. The 2D MWIR temperature maps show the device before and after the resistive switching. The entire device area warms up before the switching. After the switching, a hot (above T_c) localized filament forms. (e) Maximum temperature vs normalized current extracted from the MWIR maps. We note that the optical reflectivity (a) and IR emission measurements (d) are performed in two different setups, and, hence, the current ranges are not exactly the same.

Optical measurements show no changes at applied currents below I_{th}. As soon as the current drives the device into the NDR region, however, the reflectivity changes abruptly [Fig. 3(b)] and a distinct filamentary pattern, percolating between the electrodes, appears in the images [Fig. 3(a)]. Filamentary switching is a very common phenomenon that is observed in a variety of systems [2,3,21,47–50], extending far beyond IMT materials. In our case, the important point is that the filament has a lower optical reflectivity, which, according to our equilibrium reflectivity measurements [Fig. 1(b)], implies that the IMT is triggered during the resistive switching. The quantitative comparison between Figs. 1(b) and 3 (and Fig. 4) is, however, not feasible because of the different measurement setups. Thus, we find that passing a sufficiently large dc current drives V_3O_5 into the high-temperature metallic phase even when the base experiment temperature is 120 K below T_c. The formation of a filament is also clearly visible in the MWIR thermal mapping [Fig. 3(d)]. The MWIR microscopy reveals that after switching the filament temperature varies between 415 and 450 K, depending on the applied current. This is above the T_c of V_3O_5. Thus, the IR measurements present direct evidence that Joule heating as opposed to electrostatic doping drives the IMT triggering in V_3O_5. Unlike optical reflectivity that shows no significant contrast change prior to switching, the MWIR temperature mapping allows studying the preswitching temperature distribution in the device. We find that, before the switching, Joule heating warms up the entire device area, not just the localized area where the filament eventually forms. Right before the switching, the device temperature reaches only 330 K, i.e., far below T_c. The preswitching temperature distribution along the device width, however, is not exactly uniform: The edges of the device are about 10 K colder than the device center. Because of the steep resistance variation with temperature, small Joule heating inhomogeneity is expected to produce a substantial current "focusing," which makes Joule heating even more inhomogeneous, eventually leading to a thermal runaway. Indeed, we observe that the temperature of the

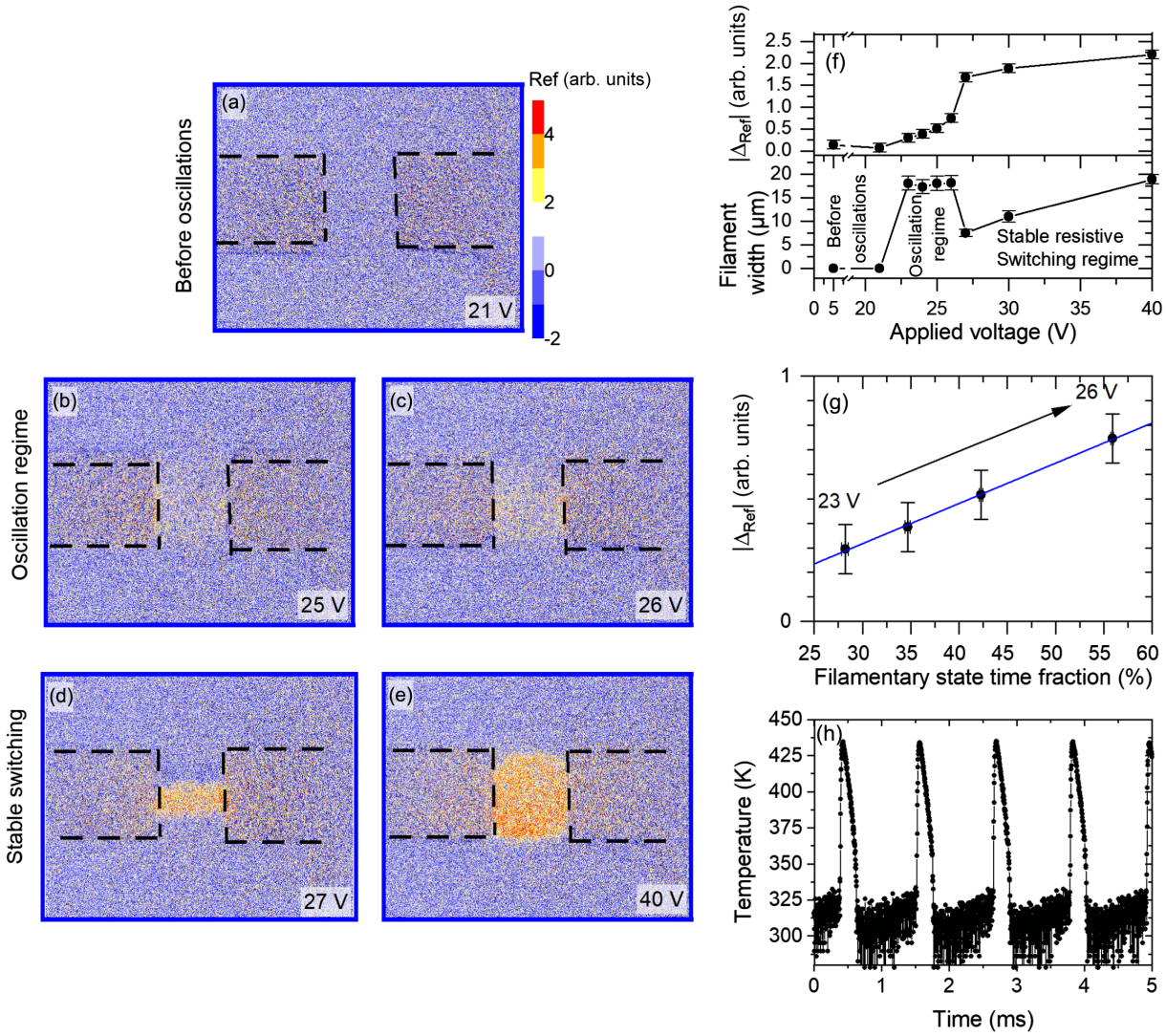

FIG. 4. Optical imaging of the self-oscillation regime in V_3O_5. (a)–(e) Differential contrast images of the resistive switching in V_3O_5 acquired at different voltages, corresponding to the homogeneous regime before oscillations in (a), the oscillation regime in (b) and (c), and during the stable resistive switching regime after the oscillations in (d) and (e). The low-temperature phase is in blue, and the high-temperature phase is in orange. The appearance of a wide low-intensity filament can be seen in the oscillation regime. (f) Applied voltage dependence of the maximum intensity and width of the filament. (g) Intensity of the reflectivity change vs time fraction spent in the filamentary state during the oscillation regime. The time spent in the filamentary state is extracted from the electrical measurement for each voltage (see Supplemental Material [46] for details). (h) Temperature vs time extracted from time-resolved IR measurements in the self-oscillation regime The temperature changes between 325 and 430 K each oscillation cycle.

device abruptly "jumps" by nearly 90 K at the threshold current [Fig. 3(e)]. Because the thermal runaway begins deep within the insulating phase (at 330 K), we conclude that the switching is not directly initiated by the resistance nonlinearities associated with the IMT. Instead, the VRS in V_3O_5 presents an intermediate case between the switching in NbO_2 [26] and in VO_2 [5,20]. Similar to NbO_2, in V_3O_5 the switching is initiated by a thermal instability driven by the nonlinear resistance vs temperature dependence. On the other hand, as in VO_2, the V_3O_5 properties after the switching, including the filament's size, resistance, temperature, etc., are a consequence of the resistance change across the T_c by Joule heating. A key feature of this large decrease of the filament resistance is to quench further thermal runaway, thus preserving the integrity of the device.

Optical imaging and time-resolved IR measurements in the V_3O_5 devices in the self-oscillation regime imply that the phase transition is triggered within each oscillation period. We acquired optical images [Figs. 4(a)–4(e)] using 55 ms exposure time, which corresponds to temporal averages of 38–55 oscillation events per image depending on the voltage bias (oscillation frequency of 0.7–1 kHz). When the applied bias drives the V_3O_5 device into the oscillation regime, a wide but low-intensity filament

appears in the images [Figs. 4(b) and 4(c)]. Because this filament corresponds to the optical reflectivity change, we can immediately conclude that V_3O_5 in the oscillation regime undergoes the phase transition following the same argument as in the case of static resistive switching (see the discussion in the previous paragraph). As the bias is increased, causing faster oscillation, the reflectivity change becomes more intense, but the filament width remains unchanged. Large bias drives the device out of the oscillation regime and induces a stable resistive switching. At the same time, the wide low-intensity filament abruptly collapses into a narrow high-intensity filament which continues to widen with further bias increase [Figs. 4(d)–4(f)], resembling the dc switching presented earlier. The filament intensity during the oscillations shows a linear correlation with the time spent in the low-resistance state as inferred from the electrical measurements [Fig. 4(g)]. This implies that the observed filament is due to the temporal averaging in the microscope camera. Therefore, this implies that the device persistently oscillates between two extreme states: filamentary with the V_3O_5 in the low-resistance state and homogeneous nonfilamentary V_3O_5 in its high resistance. This conclusion is further supported by the fact that the width of the low-intensity filament during the oscillations is approximately the same as the filament width in the stable switching regime at the same current as the peak current during the oscillation [compare Figs. 4(c) and 4(e)].

Because the filament during the oscillation is wide, it generates enough IR emission for single-shot time-resolved measurements. This allows us to probe the instantaneous temperature of the device without averaging [Fig. 4(h)]. We find that the V_3O_5 temperature oscillates between 315 K (deep in the insulating state) and 430 K (well above T_c). At the beginning of each oscillation, the temperature gradually rises from 315 to 330 K within the first 600 μs. Then, the temperature abruptly increases to 430 K, reaching T_c in about 7 μs. This abrupt temperature change provides additional support to our earlier conclusion that the thermal runaway starting deep within the insulating state is responsible for initiating the VRS in V_3O_5. After reaching the maximum temperature in the oscillating cycle, the temperature begins to rapidly decrease to 350 K (i.e., well below T_c) and then abruptly jumps to 315 K, and the cycle repeats. The final temperature jump could potentially be due to two possible scenarios: uniform cooling of the active area vs shrinking width of the hot filament. The finite spatial resolution of high-speed IR detector does not allow distinguishing between these two scenarios. Nevertheless, our IR measurements show that the thermal runaway in V_3O_5 is extremely fast, allowing for over a 100 K temperature change on a timescale much shorter than the oscillation period (10 vs 1000 μs). The optical reflectivity shows that a device-wide metallic phase filament is created and annihilated every oscillation cycle.

Because the thermal timescale associated with the VRS in V_3O_5 greatly exceeds that of the self-oscillation period, we investigate the limiting factors governing the oscillation speed using numerical simulations. We find that the dynamics of successive creation and annihilation of the filament in the self-oscillation regime is governed primarily by the electrical "inertia" of the circuit, i.e., how fast voltage or current builds up and discharges through the V_3O_5 device. We study the same circuit as in the experiments: a series resistor and a parallel capacitor connected to a V_3O_5 device. The V_3O_5 device is simulated using a resistor network (see Supplemental Material [46]), which is capable of capturing the filament formation [2,11,13,51,52]. The series capacitor and the parallel resistor are treated as lumped elements. The physics of the system is modeled using coupled time-dependent electrical and thermal equations described elsewhere [53]. Similar to the experiment, we find that, under a certain voltage bias, the V_3O_5 device oscillates between low- and high-resistance states and that a wide filament, having a temperature above T_c, forms every oscillation cycle (Fig. 5). The simulations show that the maximum dissipated power [Fig. 4(d)] lags behind the onset of the filament formation (Fig. 5, map γ). This lag is due to the capacitor discharge when the V_3O_5 device switches into the low-resistance state. The discharge does not occur instantaneously due to the *RC* time constant of the circuit. When the voltage on the capacitor reaches the threshold to initiate the VRS in V_3O_5, the discharging capacitor produces a delayed power surge, leading to the sudden formation of a very wide metallic filament in the V_3O_5, similar to the experimental observations (see Fig. 3). Interestingly, there is also a small lag between the maximum dissipated power and the maximum temperature of the device (map ε). A similar lag can also be observed between the minimum power (map λ) and the minimum temperature (map α) (see Supplemental Material [46]). Those temperature lags are due to the thermal inertia of the device, i.e., how fast the device can heat up or cool down upon a sudden change of the dissipated power. Although the oscillation frequency in our model, as in the experiment, is mainly governed by the capacitor charging or discharging rate, there could be a situation when the *RC* time constant is small and the thermal inertia becomes the dominant factor determining the oscillation behavior. As long as the *RC* time constant is larger than the thermal time constant, the oscillation regime persists [28]. In our simulations, the temperature lag is about 20 times shorter than the oscillation period; therefore, the oscillation frequency could be increased substantially by controlling the interplay between the electrical and thermal inertias.

In summary, we demonstrate that V_3O_5 thin film exhibits volatile resistive switching both in static and in fast spiking oscillatory modes. This switching can be induced at room temperature, more than 120 K below the equilibrium IMT

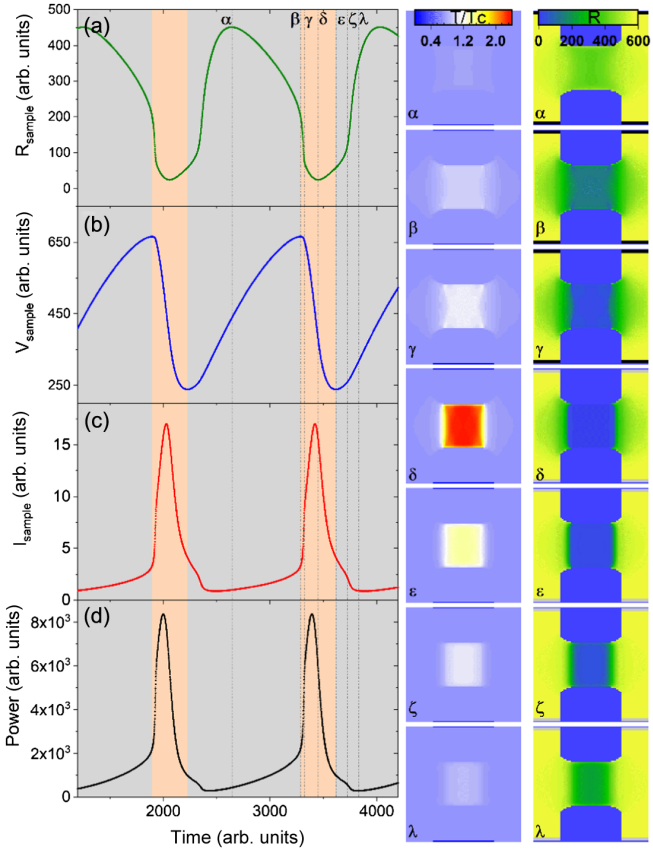

FIG. 5. Simulation of the filament formation and dissolution during the oscillations. Time dependence of (a) resistance, (b) voltage, (c) current, and (d) power simulated with a resistor network during the oscillation regime (see Supplemental Material [46] for details). The gray (orange) background corresponds to the charge (discharge) of the capacitance. Resistance and temperature maps "α" correspond to the device in the insulating state. Maps "β" correspond to the initiation of the filament when the device begins switching into a low-resistance state. Maps "γ" correspond to the device in the switched state when a high conductive filament is formed. The filament temperature is just above T_c. Maps "δ" correspond to the device in the switched state at its minimum resistance and when the maximum current is reached, just after the maximum power is reached. The filament is wider than in maps γ, and the filament temperature increases. Maps "ε" correspond to the device in a switched state when the capacitor is completely discharged. The resistance starts to increase as the filament narrows. The temperature is above T_c. Maps "ζ" correspond to the device in a switched state but in a cooler state. The temperature, although still above T_c, is decreasing, and the filament continues to narrow. Maps "λ" correspond to the device just before the relaxed state. The device cools down to T_c, and the filament narrows.

temperature of V_3O_5. Using a combination of transport, optical, and IR measurements, we show that the resistive switching is initiated in the insulating state by a thermal runaway that eventually triggers the IMT resulting in the formation of a percolating metallic-phase filament. The VRS could be induced on a short timescale, enabling fast filament creation and annihilation during each cycle in the oscillation regime. Because of the low resistivity of V_3O_5 in the insulating state (approximately 10^{-2} $\Omega \cdot$ cm) the phase transition can be driven far below T_c without causing device degradation. As a consequence, the power needed for the switching uses moderate voltages (i.e., low electric fields) without inducing ion migration and/or dielectric breakdown. This feature may be important for potential applications, since V_3O_5 devices may have a better endurance than VO_2, whose extremely large insulating state resistivity ($>10^1$ $\Omega \cdot$ cm) often leads to device breakdown before the electric triggering of the IMT. In addition, the T_c of V_3O_5 is much lower compared to NbO_2, 420 vs 1080 K. This implies that the resistive switching in V_3O_5 has a substantially better energy efficiency than NbO_2. Overall, V_3O_5 displays a similar set of functionalities as VO_2 and NbO_2 (transitions in resistivity and optical reflectivity, resistive switching, fast spiking behavior). Because of its energy efficiency, V_3O_5 could further improve a wide range of potential applications based on the IMT materials.

This collaborative work was supported as part of the Air Force Office of Scientific Research under Grant No. FA9550-20-1-0242. R. R. is supported by French ANR "MoMA" Project No. ANR-19-CE30-0020. The fabrication of the devices was performed at the San Diego Nanotechnology Infrastructure (SDNI) of UCSD, a member of the National Nanotechnology Coordinated Infrastructure, which is supported by the National Science Foundation (Grant No. ECCS-1542148). The IR measurements were performed by using an *infrascope instrument* at the Quantum Focus Instrument facility with the help of C.-P. Li.

[1] G. Mazza, A. Amaricci, M. Capone, and M. Fabrizio, *Field-Driven Mott Gap Collapse and Resistive Switch in Correlated Insulators*, Phys. Rev. Lett. **117**, 176401 (2016).

[2] P. Stoliar, M. Rozenberg, E. Janod, B. Corraze, J. Tranchant, and L. Cario, *Nonthermal and Purely Electronic Resistive Switching in a Mott Memory*, Phys. Rev. B **90**, 045146 (2014).

[3] Y. Kalcheim, A. Camjayi, J. del Valle, P. Salev, M. Rozenberg, and I. K. Schuller, *Non-Thermal Resistive Switching in Mott Insulator Nanowires*, Nat. Commun. **11**, 2985 (2020).

[4] A. Camjayi, C. Acha, R. Weht, M. G. Rodríguez, B. Corraze, E. Janod, L. Cario, and M. J. Rozenberg, *First-Order Insulator-to-Metal Mott Transition in the Paramagnetic 3D System* $GaTa_4Se_8$, Phys. Rev. Lett. **113**, 086404 (2014).

[5] A. Zimmers, L. Aigouy, M. Mortier, A. Sharoni, S. Wang, K. G. West, J. G. Ramirez, and I. K. Schuller, *Role of Thermal Heating on the Voltage Induced Insulator-Metal Transition in* VO_2, Phys. Rev. Lett. **110**, 056601 (2013).

[6] P. Markov, R. E. Marvel, H. J. Conley, K. J. Miller, R. F. Haglund, and S. M. Weiss, *Optically Monitored Electrical Switching in* VO_2, ACS Photonics **2**, 1175 (2015).

[7] N. A. Butakov, M. W. Knight, T. Lewi, P. P. Iyer, D. Higgs, H. T. Chorsi, J. Trastoy, J. Del Valle Granda, I. Valmianski, C. Urban, Y. Kalcheim, P. Y. Wang, P. W. C. Hon, I. K. Schuller, and J. A. Schuller, *Broadband Electrically Tunable Dielectric Resonators Using Metal–Insulator Transitions*, ACS Photonics **5**, 4056 (2018).

[8] I. H. Inoue and A. Sawa, *in Functional Metal Oxides* (Wiley, New York, 2013), pp. 443–463.

[9] M. Coll *et al.*, *Towards Oxide Electronics: A Roadmap*, Appl. Surf. Sci. **482**, 1 (2019).

[10] P. Salev, J. del Valle, Y. Kalcheim, and I. K. Schuller, *Giant Nonvolatile Resistive Switching in a Mott Oxide and Ferroelectric Hybrid*, Proc. Natl. Acad. Sci. U.S.A. **116**, 8798 (2019).

[11] P. Stoliar, J. Tranchant, B. Corraze, E. Janod, M.-P. Besland, F. Tesler, M. Rozenberg, and L. Cario, *A Leaky-Integrate-and-Fire Neuron Analog Realized with a Mott Insulator*, Adv. Funct. Mater. **27**, 1604740 (2017).

[12] M. D. Pickett, G. Medeiros-Ribeiro, and R. S. Williams, *A Scalable Neuristor Built with Mott Memristors*, Nat. Mater. **12**, 114 (2013).

[13] C. Adda, L. Cario, J. Tranchant, E. Janod, M.-P. Besland, M. Rozenberg, P. Stoliar, and B. Corraze, *First Demonstration of "Leaky Integrate and Fire" Artificial Neuron Behavior on* $(V_{0.95}Cr_{0.05})_2O_3$ *Thin Film*, MRS Commun. **8**, 835 (2018).

[14] J. del Valle, J. G. Ramírez, M. J. Rozenberg, and I. K. Schuller, *Challenges in Materials and Devices for Resistive-Switching-Based Neuromorphic Computing*, J. Appl. Phys. **124**, 211101 (2018).

[15] J. Feldmann, N. Youngblood, C. D. Wright, H. Bhaskaran, and W. H. P. Pernice, *All-Optical Spiking Neurosynaptic Networks with Self-Learning Capabilities*, Nature (London) **569**, 208 (2019).

[16] Y. Wang, K.-M. Kang, M. Kim, H.-S. Lee, R. Waser, D. Wouters, R. Dittmann, J. J. Yang, and H.-H. Park, *Mott-Transition-Based RRAM*, Mater. Today **28**, 63 (2019).

[17] H. S. Lee, S. G. Choi, H.-H. Park, and M. J. Rozenberg, *A New Route to the Mott-Hubbard Metal-Insulator Transition: Strong Correlations Effects in* $Pr_{0.7}Ca_{0.3}MnO_3$, Sci. Rep. **3**, 1704 (2013).

[18] J. C. Gonzalez-Rosillo, S. Catalano, I. Maggio-Aprile, M. Gibert, X. Obradors, A. Palau, and T. Puig, *Nanoscale Correlations between Metal–Insulator Transition and Resistive Switching Effect in Metallic Perovskite Oxides*, Small **16**, 2001307 (2020).

[19] Z. Yang, C. Ko, and S. Ramanathan, *Oxide Electronics Utilizing Ultrafast Metal-Insulator Transitions*, Annu. Rev. Mater. Res. **41**, 337 (2011).

[20] S. Kumar, M. D. Pickett, J. P. Strachan, G. Gibson, Y. Nishi, and R. S. Williams, *Local Temperature Redistribution and Structural Transition During Joule-Heating-Driven Conductance Switching in* VO_2, Adv. Mater. **25**, 6128 (2013).

[21] E. Janod, J. Tranchant, B. Corraze, M. Querré, P. Stoliar, M. Rozenberg, T. Cren, D. Roditchev, V. T. Phuoc, M.-P. Besland, and L. Cario, *Resistive Switching in Mott Insulators and Correlated Systems*, Adv. Funct. Mater. **25**, 6287 (2015).

[22] P. Diener, E. Janod, B. Corraze, M. Querré, C. Adda, M. Guilloux-Viry, S. Cordier, A. Camjayi, M. Rozenberg, M. P. Besland, and L. Cario, *How a dc Electric Field Drives Mott Insulators Out of Equilibrium*, Phys. Rev. Lett. **121**, 016601 (2018).

[23] S. Kumar, Z. Wang, N. Davila, N. Kumari, K. J. Norris, X. Huang, J. P. Strachan, D. Vine, A. L. D. Kilcoyne, Y. Nishi, and R. S. Williams, *Physical Origins of Current and Temperature Controlled Negative Differential Resistances in* NbO_2, Nat. Commun. **8**, 1 (2017).

[24] X. Liu, S. Li, S. K. Nandi, D. K. Venkatachalam, and R. G. Elliman, *Threshold Switching and Electrical Self-Oscillation in Niobium Oxide Films*, J. Appl. Phys. **120**, 124102 (2016).

[25] G. A. Gibson, S. Musunuru, J. Zhang, K. Vandenberghe, J. Lee, C.-C. Hsieh, W. Jackson, Y. Jeon, D. Henze, Z. Li, and R. S. Williams, *An Accurate Locally Active Memristor Model for S-Type Negative Differential Resistance in NbOx*, Appl. Phys. Lett. **108**, 023505 (2016).

[26] C. Funck, S. Menzel, N. Aslam, H. Zhang, A. Hardtdegen, R. Waser, and S. Hoffmann-Eifert, *Multidimensional Simulation of Threshold Switching in* NbO_2 *Based on an Electric Field Triggered Thermal Runaway Model*, Adv. Electron. Mater. **2**, 1600169 (2016).

[27] S. Slesazeck, H. Mähne, H. Wylezich, A. Wachowiak, J. Radhakrishnan, A. Ascoli, R. Tetzlaff, and T. Mikolajick, *Physical Model of Threshold Switching in* NbO_2 *Based Memristors*, RSC Adv. **5**, 102318 (2015).

[28] M. Herzig, M. Weiher, A. Ascoli, R. Tetzlaff, T. Mikolajick, and S. Slesazeck, *Multiple Slopes in the Negative Differential Resistance Region of* NbO_x*-Based Threshold Switches*, J. Phys. D **52**, 325104 (2019).

[29] G. Andersson, *Studies on Vanadium Oxides. I. Phase Analysis.*, Acta Chem. Scand. **8**, 1599 (1954).

[30] S. Åsbrink, *The Crystal Structure of, and Valency Distribution in the Low-Temperature Modification of* V_3O_5. *The Decisive Importance of a Few Very Weak Reflexions in a Crystal-Structure Determination*, Acta Crystallogr. Sect. B **36**, 1332 (1980).

[31] S. Åsbrink and S.-H. Hong, *Increase of X-Ray Reflection Intensities and Profile Widths at the Low- to High-*V_3O_5 *Phase Transition State*, Nature (London) **279**, 624 (1979).

[32] E. Abreu, M. Liu, J. Lu, K. G. West, S. Kittiwatanakul, W. Yin, S. A. Wolf, and R. D. Averitt, *THz Spectroscopy of* VO_2 *Epitaxial Films: Controlling the Anisotropic Properties through Strain Engineering*, New J. Phys. **14**, 083026 (2012).

[33] M. Yang, Y. Yang, B. Hong, L. Wang, K. Hu, Y. Dong, H. Xu, H. Huang, J. Zhao, H. Chen, L. Song, H. Ju, J. Zhu, J. Bao, X. Li, Y. Gu, T. Yang, X. Gao, Z. Luo, and C. Gao, *Suppression of Structural Phase Transition in* VO_2 *by Epitaxial Strain in Vicinity of Metal-Insulator Transition*, Sci. Rep. **6**, 23119 (2016).

[34] V. N. Andreev and V. A. Klimov, *Specific Features of Electrical Conductivity of* V_3O_5 *Single Crystals*, Phys. Solid State **53**, 2424 (2011).

[35] N. Kumar, A. Rúa, J. Lu, F. Fernández, and S. Lysenko, *Ultrafast Excited-State Dynamics of* V_3O_5 *as a Signature of*

a Photoinduced Insulator-Metal Phase Transition, Phys. Rev. Lett. **119**, 057602 (2017).

[36] L. Baldassarre, A. Perucchi, E. Arcangeletti, D. Nicoletti, D. Di Castro, P. Postorino, V. A. Sidorov, and S. Lupi, *Electrodynamics near the Metal-to-Insulator Transition in* V_3O_5, Phys. Rev. B **75**, 245108 (2007).

[37] F. A. Chudnovskii, E. I. Terukov, and D. I. Khomskii, *Insulator-Metal Transition in* V_3O_5, Solid State Commun. **25**, 573 (1978).

[38] V. A. Sidorov, A. Waśkowska, and D. Badurski, V_3O_5 *at High Pressure: A Possible Heavy Fermion 3d-Metal Oxide*, Solid State Commun. **125**, 359 (2003).

[39] A. Rúa, R. D. Díaz, N. Kumar, S. Lysenko, and F. E. Fernández, *Metal-Insulator Transition and Nonlinear Optical Responseof Sputter-Deposited* V_3O_5 *Thin Films*, J. Appl. Phys. **121**, 235302 (2017).

[40] B. Fisher, L. Patlagan, K. B. Chashka, C. Makarov, and G. M. Reisner, V_3O_5*: Insulator-Metal Transition and Electric-Field-Induced Resistive-Switching*, Appl. Phys. Lett. **109**, 103501 (2016).

[41] E. I. Terukov, F. A. Chudnovskii, W. Reichelt, H. Oppermann, W. Brückner, H.-P. Brückner, and W. Moldenhauer, *Investigation of the Physical Properties of* V_3O_5 *at Phase Transition with Consideration of Its Range of Homogeneity*, Phys. Status Solidi A **37**, 541 (1976).

[42] M.-H. Lee, Y. Kalcheim, J. del Valle, and I. K. Schuller, *Controlling Metal–Insulator Transitions in Vanadium Oxide Thin Films by Modifying Oxygen Stoichiometry*, ACS Appl. Mater. Interfaces **13**, 887 (2021).

[43] W. Gerstner, W. M. Kistler, R. Naud, and L. Paninski, *Neuronal Dynamics: From Single Neurons to Networks and Models of Cognition* (Cambridge University Press, Cambridge, England, 2014).

[44] M. I. Rabinovich, P. Varona, A. I. Selverston, and H. D. I. Abarbanel, *Dynamical Principles in Neuroscience*, Rev. Mod. Phys. **78**, 1213 (2006).

[45] S. O. Pearson and H. S. G. Anson, *Demonstration of Some Electrical Properties of Neon-Filled Lamps*, Proc. Phys. Soc. London **34**, 175 (1921).

[46] See Supplemental Material at http://link.aps.org/supplemental/10.1103/PhysRevX.12.011025 for information about the statistics on the oscillation regime, the analysis of the reflectivity images and IR measurements, and information about the simulations.

[47] C. Adda, B. Corraze, P. Stoliar, P. Diener, J. Tranchant, A. Filatre-Furcate, M. Fourmigué, D. Lorcy, M.-P. Besland, E. Janod, and L. Cario, *Mott Insulators: A Large Class of Materials for Leaky Integrate and Fire (LIF) Artificial Neuron*, J. Appl. Phys. **124**, 152124 (2018).

[48] Z. Wang, S. Joshi, S. E. Savel'ev, H. Jiang, R. Midya, P. Lin, M. Hu, N. Ge, J. P. Strachan, Z. Li, Q. Wu, M. Barnell, G.-L. Li, H. L. Xin, R. S. Williams, Q. Xia, and J. J. Yang, *Memristors with Diffusive Dynamics as Synaptic Emulators for Neuromorphic Computing*, Nat. Mater. **16**, 101 (2017).

[49] T. Liu, M. Verma, Y. Kang, and M. Orlowski, *Volatile Resistive Switching in* $\mathrm{Cu/TaOx}/\delta - \mathrm{Cu/Pt}$ *Devices*, Appl. Phys. Lett. **101**, 073510 (2012).

[50] W. Wang, M. Laudato, E. Ambrosi, A. Bricalli, E. Covi, Y.-H. Lin, and D. Ielmini, *Volatile Resistive Switching Memory Based on Ag Ion Drift/Diffusion Part I: Numerical Modeling*, IEEE Trans. Electron Devices **66**, 3795 (2019).

[51] F. Tesler, C. Adda, J. Tranchant, B. Corraze, E. Janod, L. Cario, P. Stoliar, and M. Rozenberg, *Relaxation of a Spiking Mott Artificial Neuron*, Phys. Rev. Applied **10**, 054001 (2018).

[52] J. del Valle, P. Salev, F. Tesler, N. M. Vargas, Y. Kalcheim, P. Wang, J. Trastoy, M.-H. Lee, G. Kassabian, J. G. Ramírez, M. J. Rozenberg, and I. K. Schuller, *Subthreshold Firing in Mott Nanodevices*, Nature (London) **569**, 388 (2019).

[53] P. Stoliar, L. Cario, E. Janod, B. Corraze, C. Guillot-Deudon, S. Salmon-Bourmand, V. Guiot, J. Tranchant, and M. Rozenberg, *Universal Electric-Field-Driven Resistive Transition in Narrow-Gap Mott Insulators*, Adv. Mater. **25**, 3222 (2013).